Simple technique for generating the perfect optical vortex

Joaquín García-García,[1] Carolina Rickenstorff-Parrao,[1] Rubén Ramos-García,[2] Víctor Arrizón,[2] and Andrey S. Ostrovsky[1,*]

[1]*Facultad de Ciencias Físico Matemáticas, Benemérita Universidad Autónoma de Puebla, Puebla 72000, Mexico*

[2]*Área de Óptica, Instituto Nacional de Astrofísica, Óptica y Electrónica, Puebla 72000, Mexico*

**Corresponding author: andreyo@fcfm.buap.mx*

Received June 24, 2014; revised August 6, 2014; accepted August 8, 2014;
posted August 12, 2014 (Doc. ID 214557); published September 5, 2014

We propose an improved technique for generating the perfect optical vortex. This technique is notable for the simplicity of its practical realization and high quality of the results. The efficiency of the proposed technique is illustrated with the results of physical experiments and an example of its application in optical trapping of small particles.

OCIS codes: (050.4865) Optical vortices; (070.6120) Spatial light modulators; (230.3720) Liquid-crystal devices; (140.7010) Laser trapping.

http://dx.doi.org/10.1364/OL.39.005305

As is well known, an optical vortex beam possesses a helical wavefront able to transfer orbital angular momentum to dielectric particles at a rate proportional to its topological charge. Thus such a beam is a very effective tool in many applications related to optical trapping and manipulation [1]. Several techniques for generating the optical vortex beam have been reported during last decade [2–12], but all of them exhibit a strong dependence of the vortex radius on the topological charge, making it difficult to obtain a high spatial accuracy and a high orbital angular momentum simultaneously. Recently, we reported a new type of optical vortex, called perfect vortex [13], whose radius is independent of topological charge and whose intensity gradient takes an extremely large value. This concept is today widely recognized by the optics community [14–25]. It was demonstrated that the perfect vortex can be approximately generated in a Fourier transforming optical system with a computer-controlled liquid-crystal (LC) spatial light modulator (SLM) working in the phase mode. Unfortunately, the original technique was very cumbersome in its practical realization because of the complex modulation of the transmission mode of the SLM used, namely a twisted nematic LC-SLM. In consequence, the quality of the generated vortex was rather poor. Here we propose an improved technique for generating the perfect optical vortex which is notable for the simplicity of its practical realization and the high quality of its results. The efficiency of the proposed technique is illustrated with the results of physical experiments and an example of its application in optical trapping of small particles.

We start recalling the definition of the perfect vortex as an optical beam with the transverse distribution of complex amplitude given by the ideal model

$$g_\nu(\rho,\theta) \equiv \delta(\rho-\rho_0)\exp(i\nu\theta), \tag{1}$$

where $\delta(\rho)$ is the Dirac δ-function, (ρ,θ) are the polar coordinates in the beam cross section, ρ_0 is the radius of the vortex, and ν is an integer, known as the topological charge of the vortex. Such a vortex can be approximately generated by means of the Fourier transforming optical system. As is well known, the complex amplitude distributions in the back (ρ,θ) and front (r,φ) focal planes of this system are related by the Fourier transform [26], i.e.,

$$U(\rho,\theta) = \int_0^\infty \int_0^{2\pi} U(r,\varphi)\exp\left[-i\frac{2\pi}{\lambda f} r\rho\cos(\theta-\varphi)\right] r\mathrm{d}r\mathrm{d}\varphi, \tag{2}$$

where λ is the wavelength of illumination and f is the focal length of the Fourier transforming lens. Then, replacing $U(\rho,\theta)$ in the inverse version of Eq. (2) by $g_\nu(\rho,\theta)$ from Eq. (1) and using the sifting property of δ-function together with the integral representation of the nth-order Bessel function of the first kind [27],

$$J_\nu(x) = \frac{i^{-\nu}}{2\pi}\int_0^{2\pi} \exp(i\nu\phi)\exp(ix\cos\phi)\mathrm{d}\phi, \tag{3}$$

one readily finds that, to obtain the perfect vortex, the input optical signal must be chosen in accordance with

$$U(r,\varphi) \propto J_\nu\left(\frac{2\pi}{\lambda f} r\rho_0\right)\exp(i\nu\varphi). \tag{4}$$

The optical signal, Eq. (4), can be obtained by means of two SLMs that modify the amplitude and the phase of illumination field, respectively. In order to use only one phase modulator, we admit the width-pulse approximation of Bessel function in Eq. (4) shown in Fig. 1 for positive value of ν and described by

$$J_\nu\left(\frac{2\pi}{\lambda f} r\rho_0\right) \approx \sum_n (-1)^{n-1}\,\mathrm{rect}\left(\frac{r-r_{\nu,n}}{\Delta r_{\nu,n}}\right), \tag{5}$$

where $\mathrm{rect}(r)$ is the rectangle function, $r_{\nu,n}$ is the nth root of equation

$$\frac{d}{dr}J_\nu\left(\frac{2\pi}{\lambda f} r\rho_0\right) = 0, \tag{6}$$

and

$$\Delta r_{\nu,n} \propto \frac{|J_\nu(2\pi r_{\nu,n}\rho_0/\lambda f)|}{J_\nu(2\pi r_{\nu,1}\rho_0/\lambda f)}. \tag{7}$$

Then, the field given by Eq. (4) can be approximately reproduced transmitting the uniform plane wave through

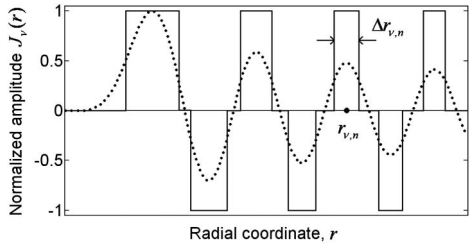

Fig. 1. Width-pulse approximation (solid curve) of Bessel function (dotted curve).

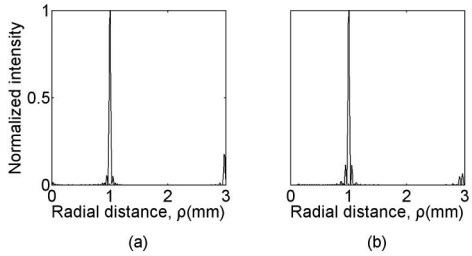

Fig. 2. Intensity distribution computed in accordance with Eq. (11): (a) $\nu = 1$ and (b) $\nu = 10$.

a phase screen formed by a set of concentric rings with the total amplitude transmittance

$$T(r,\varphi) = \exp\left(i\frac{2\pi}{\lambda f}x_0' x\right)\sum_n \mathrm{rect}\left(\frac{r-r_{\nu,n}}{\Delta r_{\nu,n}}\right)\exp[i\nu(\varphi-\varphi_{\nu,n})], \tag{8}$$

which are separated by a set of complementary concentric rings with the total amplitude transmittance

$$T'(r,\varphi) = \exp\left(-i\frac{2\pi}{\lambda f}x_0' x\right)\left[1-\sum_n \mathrm{rect}\left(\frac{r-r_{\nu,n}}{\Delta r_{\nu,n}}\right)\right]. \tag{9}$$

In Eq. (8) $\varphi_{\nu,n}$ takes value 0 for odd n and π/ν for even n. The phase factors $\exp(\pm i2\pi x_0' x/\lambda f)$ in Eqs. (8) and (9) are introduced to separate the result of useful modulation from the parasite light passed through the spaces between modulating rings, so that the generated vortex will be centered at the off axis position $(x' = -x_0', y' = 0)$. Since the modulation of the optical signal specified by Eqs. (8) and (9) has unity modulus in all the points, it can be effectively realized by means of a commercial computer controlled LC-SLM operating in phase-only modulation mode.

Using Eqs. (2)–(8), one finds the signal centered at the point $(x' = -x_0', y' = 0)$ of the output plane of the Fourier transforming optical system

$$U(\rho,\theta) = \exp(i\nu\theta)\sum_n (-1)^{n-1}\int_{r_{\nu,n}-\Delta r_{\nu,n}/2}^{r_{\nu,n}+\Delta r_{\nu,n}/2} J_\nu\left(\frac{2\pi}{\lambda f}r\rho\right) r\mathrm{d}r. \tag{10}$$

It is not out of place to mention here that the negative value of the topological charge ν in Eq. (10) can be obtained by simple inverting the sign of the phase in Eq. (8).

Taking into account that the exponential factor in Eq. (10) exactly reproduces the required helical wavefront, we computed only the intensity distribution

$$I(\rho) = \left|\sum_{n=1}^{N}(-1)^{n-1}\int_{r_{\nu,n}-\Delta r_{\nu,n}/2}^{r_{\nu,n}+\Delta r_{\nu,n}/2} J_\nu\left(\frac{2\pi}{\lambda f}r\rho\right) r\mathrm{d}r\right|^2, \tag{11}$$

where N is a truncating parameter. The results of computation for $\rho_0 = 1$ mm, $N = 20$, and two different values of ν (1 and 10) are shown in Fig. 2 (for the sake of simplicity, in both cases the factor $2\pi/\lambda f$ was set equal to unity). These results can be recognized as a rather good approximation of the perfect vortices. As a whole, the results of the computation demonstrate the consistence of the approximation given by Eq. (5).

To verify the proposed technique in practice, we realized two physical experiments using the setup shown in Fig. 3. In these experiments we employed the computer-controlled phase-only reflective LC-SLM Pluto-Vis from HoloEye Photonics AG with 1920 × 1080 pixel resolution and 8.0 μm pixel pitch. The control video signals were generated using Matlab routines and displayed onto the LC panel with an accuracy of 256 gray levels. As the light source we used a low power He–Ne laser (633 nm). To register the results, we employed a CCD camera.

In the first experiment we displayed onto the LC-SLM the control video signals of the form $\exp(i\nu\varphi)$ with different values of ν and registered the superposition of the modulated light with an inclined plane wave from the same laser source. The control video signals and registered interference patterns are shown in Fig 4. The fork structure of the interference fringes in Fig. 4(b), with the difference in the number of fringes in the bottom and the top of the interference patterns equal to ν, testifies evidently to the presence of optical vortex. This result ensures the accuracy in the following experiments where we deal only with the intensity measurements.

In the second experiment we generated the control video signals in accordance with Eqs. (8) and (9) to create the perfect vortices of radius $\rho_0 = 1.5$ mm and different values of topological charge. To display effectively the control signals onto the active area of the LC-SLM, we truncated the number of modulating rings by number N depending on the value of topological charge. An example of generated control video signal corresponding to $\nu = 10$ and $N = 20$ is depicted in Fig. 5. The intensity distributions of the generated vortices shown in Fig. 6 exhibit a sharp intensity profile with the radius independent of the topological charge. The discernible increase of the principal ring width and of the parasite ring's

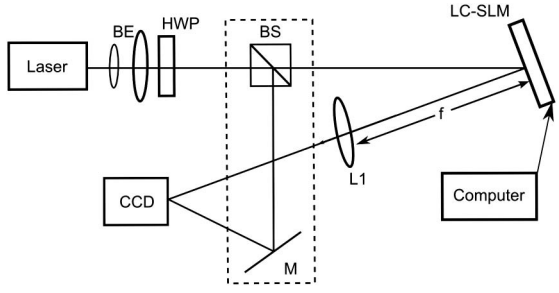

Fig. 3. Experimental setup used for generating the perfect vortex: BE, beam expander; HWP, half-wave plate; BS, beam splitter; and L, lens; M, mirror.

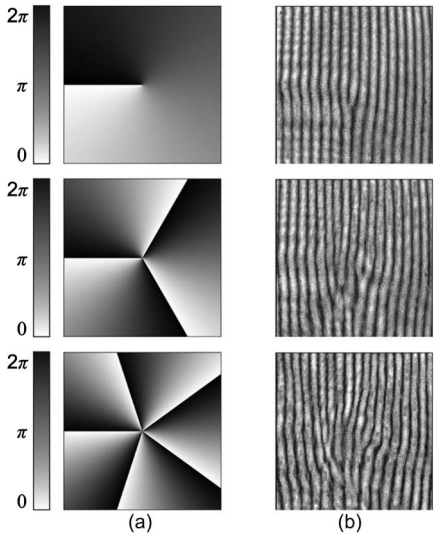

Fig. 4. (a) Control video signals and (b) registered interference patterns in the first experiment for values $\nu = 1$, $\nu = 3$, and $\nu = 5$.

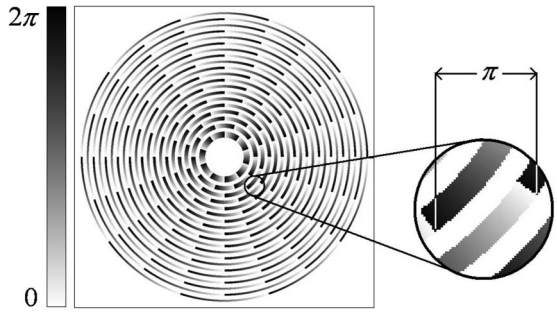

Fig. 5. Example of the control video signal for $\rho_0 = 1$ mm, $\nu = 10$ and $N = 20$ (for better clearness the spatial carrier is omitted).

visibility can be explained by the systematic error because of the accepted width-pulse approximation of Bessel function. It is obvious that the minimum attainable size of the generated vortex is limited by the effective width of the principal vortex ring which was about 0.18 mm in the case of Fig. 6(d).

To illustrate the possible applications of the proposed technique, we have realized one more experiment in which the generated perfect optical vortex with a radius

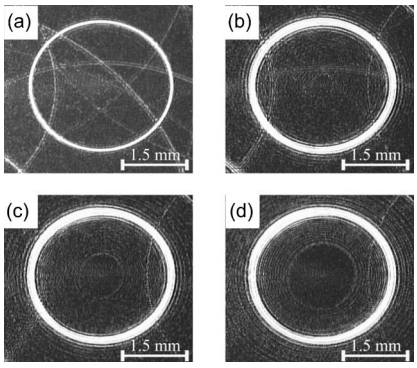

Fig. 6. Generated vortices with radius $\rho_0 = 1.5$ mm and topological charge: (a) $\nu = 1$; (b) $\nu = 20$; (c) $\nu = 40$; and (d) $\nu = 60$.

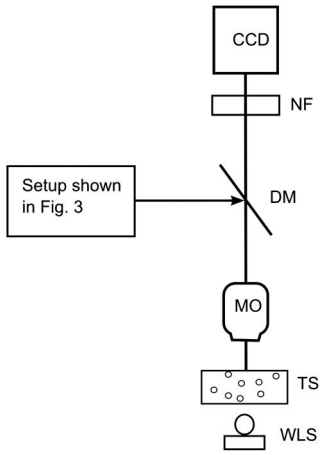

Fig. 7. Optical trapping setup: WLS, white light source; TS, test specimen; MO, microscope objective; DM, dichroic mirror; and NF, neutral filter.

of 0.3 mm and topological charge of 15 was employed for trapping silica particles of 2.5 μm diameter suspended in water. The optical setup used in this experiment is shown in Fig. 7. It consists of two parts: the first one is the same as shown in Fig. 3; the second one is a typical optical tweezers setup. The test specimen with silica particles was placed in the focal plane of the microscope objective with 1.4 N.A. and 100× magnification which projects the white light source onto the CCD camera through the dichroic mirror and neutral filter. To provide the reliable interaction between generated vortex and silica particles, in this experiment we used a high power (1 W) DPSS laser (532 nm). The time evolution of the trapping process using the perfect vortex is shown in Fig. 8. As can be seen in this figure, the exposed silica particles appear to be stably trapped at the vortex edge after three minutes. Moreover, they rotate about the vortex center with the velocity proportional to the topological charge.

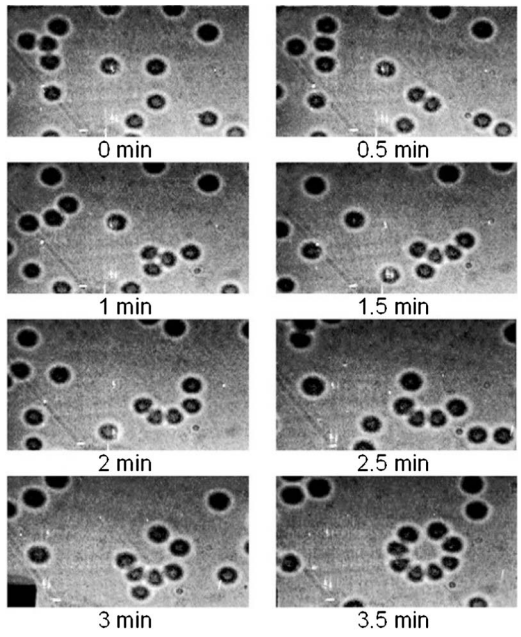

Fig. 8. Temporal sequence of optical trapping silica particles using the perfect vortex generated by means of the proposed technique.

In conclusion, an improved technique for generating the perfect vortex based on the width-pulse approximation of Bessel function is proposed. Comparing this technique with the one reported in our previous publication [13], we find that it is notable for the simplicity of its practical realization and high quality of the provided results. We consider that this technique can be widely adopted in optical trapping and manipulation of small particles.

This work was supported by the Benemérita Universidad Autónoma de Puebla (project VIEP OSA.EXC-14) and by the National Council for Science and Technology of Mexico (projects CB-165142 and CB-153463).

References

1. A. M. Yao and M. J. Padgett, Adv. Opt. Photon. **3**, 161 (2011).
2. C.-S. Guo, X. Liu, J.-L. He, and H.-T. Wang, Opt. Express **12**, 4625 (2004).
3. C.-S. Guo, X. Liu, X.-Y. Ren, and H.-T. Wang, J. Opt. Soc. Am. A **22**, 385 (2005).
4. J. Lin, X.-C. Yuan, S. H. Tao, and R. E. Burge, Opt. Lett. **31**, 1600 (2006).
5. V. Arrizón, S. Chávez-Cerda, U. Ruiz, and R. Carrada, Opt. Express **15**, 16748 (2007).
6. J. Chen, X.-C. Yuan, X. Zhao, Z. L. Fang, and S. W. Zhu, Opt. Lett. **34**, 3289 (2009).
7. R. Valsilyeu, A. Dudley, N. Khilo, and A. Forbes, Opt. Express **17**, 23389 (2009).
8. V. Arrizón, D. Sánchez-de-la-Llave, U. Ruiz, and G. Méndez, Opt. Lett. **34**, 1456 (2009).
9. J. Chen, X. Zhao, Z. Fang, and X.-C. Yuan, J. Opt. Soc. Am. A **27**, 935 (2010).
10. J. Chen, Y. Yu, and F. Wang, Chin. Opt. Lett. **9**, 011402 (2011).
11. A. Dudley and A. Forbes, J. Opt. Soc. Am. A **29**, 567 (2012).
12. A. Calatayud, J. A. Rodrigo, L. Remón, W. D. Furlan, G. Cristóbal, and J. A. Monsoriu, Appl. Phys. B **106**, 915 (2012).
13. A. S. Ostrovsky, C. Rickenstorff-Parrao, and V. Arrizón, Opt. Lett. **38**, 534 (2013).
14. M. Z. Chen, M. Mazilu, Y. Arita, E. M. Wright, and K. Dholakia, Opt. Lett. **38**, 4919 (2013).
15. M. D. Williams, M. M. Coles, K. Saadi, D. S. Bradshaw, and D. L. Andrews, Phys. Rev. Lett. **111**, 153603 (2013).
16. M. D. Williams, M. M. Coles, D. S. Bradshaw, and D. L. Andrews, Phys. Rev. A **89**, 033837 (2014).
17. D. L. Andrews, J. Nanophoton. **8**, 081599 (2014).
18. T. Roger, J. J. F. Heitz, E. M. Wright, and D. Faccio, Sci. Rep. **3**, 3491 (2013).
19. Z. H. Li, M. N. Zhang, X. Li, C. X. Liu, and C. F. Cheng, Chin. Phys. Lett. **30**, 104206 (2013).
20. C. Hernandez-Garcia, A. Picon, J. San Roman, and L. Plaja, Phys. Rev. Lett. **111**, 083602 (2013).
21. P. R. Gill, Opt. Lett. **38**, 2074 (2013).
22. C. He and S.-J. Huang, J. Optoelectron. Laser **24**, 2440 (2013).
23. C. He, S. Huang, T. Gu, and T. Wang, Chin. J. Lasers **41**, 0309003 (2014).
24. S. J. Huang, C. He, and T. Y. Wang, J. Opt. **16**, 035402 (2014).
25. G. Assanto, A. A. Minzoni, and N. F. Smyth, Phys. Rev. A **89**, 013827 (2014).
26. J. W. Goodman, *Introduction to Fourier Optics* (McGraw-Hill, 1996).
27. G. B. Arfken and H. J. Weber, *Mathematical Methods for Physicists*, 3rd ed. (Harcourt/Academic, 2001).